

Article

A Novel Wideband Magnetolectric Dipole Antenna with Circular Polarization Applied to CubeSat

Bruno Matias de Sousa¹ , José Garibaldi Duarte Júnior² , Valdemir Praxedes da Silva Neto³ 

¹Graduação em Engenharia Elétrica, Federal University of Rio Grande do Norte, Natal, RN, Brazil, bruno.matias.017@ufrn.edu.br

²Programa de Pós-Graduação em Engenharia Elétrica e Computação, Federal University of Rio Grande do Norte, Natal, RN, Brazil, garibaldijrn@gmail.com

³Departamento de Engenharia de Comunicações, Federal University of Rio Grande do Norte, Natal, RN, Brazil, valdemir.praxedes@ufrn.br

Abstract— In this work a broadband Magnetolectric (ME) dipole antenna for the Global Navigation Satellite System (GNSS) applied to nanosatellites is proposed. The antenna consists of a reflective cavity with open walls containing four gaps to enhance the axial ratio (AR) bandwidth. Additionally, it includes two ME dipoles formed by two pairs of vertical and horizontal copper plates, one of which is trapezoidal and a T- Γ -shaped cross-feeding structure. A prototype was designed and subsequently manufactured and measured. The experimentally obtained results exhibit consistent agreement with simulated outcomes, demonstrating that the antenna has a wide impedance bandwidth of 111.36% from 1.13 GHz to 1.62 GHz for the Voltage Standing Wave Ratio (VSWR) ≤ 2 and a 3 dB AR bandwidth of 120.45% from 1.10 GHz to 1.63 GHz. Within this range, high gain (≥ 8.5 dBi) and high radiation efficiency (90%) can be achieved. Furthermore, the antenna exhibits right-hand circular polarization (RHCP) and possesses good unidirectional radiation characteristics with a high front-to-back ratio (≥ 20 dB).

Index Terms— CubeSat, GNSS, Magnetolectric Dipole, Wideband Antenna

I. INTRODUCTION

Since the concept of magnetolectric (ME) dipole antennas, as proposed by [1], they have been widely employed in the aerospace domain, particularly in small satellites, owing to their performance and physical characteristics. These antennas exhibit a low radiation pattern in the back lobe, high gains, and a compact antenna profile that contributes to improved motion dynamics of these minisatellites compared to conventional physical antennas. Additionally, there is a heightened susceptibility to damages such as radiation, space debris, and micrometeoroids [2].

A typical ME dipole antenna is the junction of a pair of vertically positioned metal plates short-circuited in a quarter-wave at one end to produce a magnetic dipole and two horizontally positioned metal plates thus producing an electric dipole orthogonal to the magnetic dipole [3]. In this context, circular polarization (CP) radiation is usually generated in the traditional way using two orthogonal dipoles of half the wavelength, fed by sources of equal magnitude and with a phase difference of 90 degrees between them [4]. In addition, the interference of the two fields produces a radiation pattern in

which the broadside gain is high and the back lobe gain is very low. Therefore, this type of structure is perfectly suited to generating a hemispherical radiation pattern. Another parameter analyzed in this antenna is its polarization, which can be linear or circular [5].

ME dipole antennas with CP have several significant characteristics, such as greater resistance to distortion caused by multiple paths, minimization of the effects of Faraday rotation caused by the ionosphere, and reduced losses due to polarization mismatch [6]. Due to these advantages, CP antennas are becoming a fundamental technology for a variety of current and future wireless communication systems, including satellite communications, global navigation satellite systems (GNSS), mobile communications, broadcasting and TV transmission, defense systems, among others [7]. Nowadays, many CP antennas use metamaterials or active elements to reduce their size [8]. However, these types of antennas usually only work in a specific minimum GNSS band, and the vast majority have a loss of performance due to the need for control circuits required for the active elements introduced [9].

For wideband operation, conventional dipoles are replaced by modified radiators, which have wider bandwidth responses. These designs also require a double cross-feed to achieve the desired CP radiation [4]. The excitation of these antennas can be carried out using a feeding network, such as a Wilkinson power divider with a double-slot line microstrip or a T-junction power divider [10]. In general, these structures include a power divider and a quarter-wavelength stage, which usually makes the design and manufacture of the antenna more complex.

Wideband CP crossed dipole antennas with a single feed have received a significant attention recently, as due to their compactness they have relevant characteristics in relation to the half-power beamwidth (HPBW) [11]. However, CP ME dipole antennas have more useful functions compared to these antennas, as they produce a higher broadside gain and weak background radiation, which are essential for GNSS operation, and also have an axial ratio bandwidth (AR) below 3 dB [12].

As a result, several services provided by satellite navigation systems have expanded globally in the military and commercial areas [13]. Nowadays, there are four global navigation satellite systems (GNSS) around the world: the global positioning system (GPS), the Russian global navigation satellite system (GLONASS), the European Union system (Galileo) and the Chinese navigation system (Beidou), as well as other smaller private navigation systems [10]. The antennas used in GNSS applications have attracted considerable attention because they have a band with several different integrated systems, thus offering a wide range of applications in different areas. As such, an antenna designed to operate across the entire GNSS band must have a number of characteristics, including broadband, covering the frequency range from 1.164 to 1.610 GHz, emitting right-hand circularly polarized radiation (RHCP), with a wide aperture angle and a high signal-to-noise ratio. Current literature covers numerous models of wideband circularly polarized antennas developed for GNSS applications [13].

The literature describes several ME antennas with CP [4] - [14], some of which have CP radiation generated by feeders involving power dividers and phase shifters [10], increasing the complexity of manufacturing these antennas. Thus, a series of ME antennas with CP was developed with a single gamma source connected to an SMA [5] - [9]. After this, antennas with a single feed and a crossed dipole were investigated [11] - [15]. In this way, we can better explain the mechanism that generates the CP to demonstrate that a single feeder with a crossed dipole connected in parallel and its power and phase relationships are obtained by correctly choosing the lengths of the two dipoles in question [4].

Recently, alternative engineering approaches for single feed cross dipole antenna have been adopted, however, some important parameters such as AR do not fully cover the desired GNSS spectra [11] - [16]. Some of these are: A bow-tie printed dipole antenna with a crossed dipole, an impedance matching of 1.05-1.79 GHz and an AR of 1.12-1.64 GHz bandwidth were obtained [11]. A dual-band ME dipole antenna with double CP direction, with a single feeding, obtained an impedance match of (2.15-3.4) and (4-6.3) GHz and an AR of (2.5-3.35) and (5-5.7) GHz [15]. A classic wideband circularly polarized ME dipole antenna with a modified reflector cavity in which an impedance matching of 1.76-3.46 GHz and an AR of 1.68-3.55 GHz bandwidth were obtained [17]. Another antenna analyzed a crossed dipole with four parasitic plates in order to study the phase center variation and the phase center deviation to obtain a stable phase center, thus obtaining an impedance matching of 1.04-2.0 GHz and an AR of 1.1-1.88 GHz bandwidth [7]. Finally, a CP dipole antenna for GNSS application was investigated, typically a crossed dipole with a different structure on both sides. These tapered dipoles are applied to the radiator to increase the impedance bandwidth, while parasitic blade-shaped patches are added to the side of each dipole to increase the AR bandwidth. This results in an impedance match of 0.98-1.64 GHz and an AR bandwidth of 1.16-1.65 GHz [14].

In this article, the proposed antenna is a ME cross-dipole antenna with a single feed, wideband, applied to the GNSS band, and consequently circularly polarized. Its overall volume is $0.877\lambda_0 \times 0.785\lambda_0 \times 0.254\lambda_0$ (λ_0 is the wavelength of 1.385 GHz in free space). The proposed ME antenna is composed of an open cavity reflector on the sidewalls, two center-symmetric ME dipole antenna elements, one with a standard rectangular structure and the other with a trapezoidal structure, adding the inherent phase difference between the M dipole and the E dipole, the CP character can be easily achieved. A feed structure, consisting of a T-shaped pedestal and two Γ -shaped feed lines with different heights, is used to excite the antenna. Based on the simulation the bandwidth for $|S_{11}| < -10\text{dB}$, is 1.03-1.61GHz, and the bandwidth for AR less than 3 dB, is 1.16-1.65GHz which comprises the entire GNSS band for both cases. The valid bandwidth of the right-hand CP (RHCP) is 1.16 to 1.65 GHz. In addition, high peak gains (8.69 dBi), high radiation efficiencies and high front-to-back ratio (FBR) are also achieved. Therefore, the proposed wideband compact ME dipole antenna is potentially suitable for the entire GNSS band. The antenna was first characterized with ANSYS - Ansoft High Frequency Structure Simulator (HFSS), CST Studio, then verified through measurements.

II. ANTENNA DESIGN AND ANALYSES

A. Antenna Geometry

The geometry of the proposed ME dipole antenna is shown in Fig. 1. The antenna structure is made of 0.3 mm thick copper sheet. The antenna consists of an open reflector cavity, as well as a power supply generated by an SMA connector that is connected together with a T-shaped copper structure integrating two Γ -shaped feeders, thus feeding two ME dipole antenna elements of different shapes.

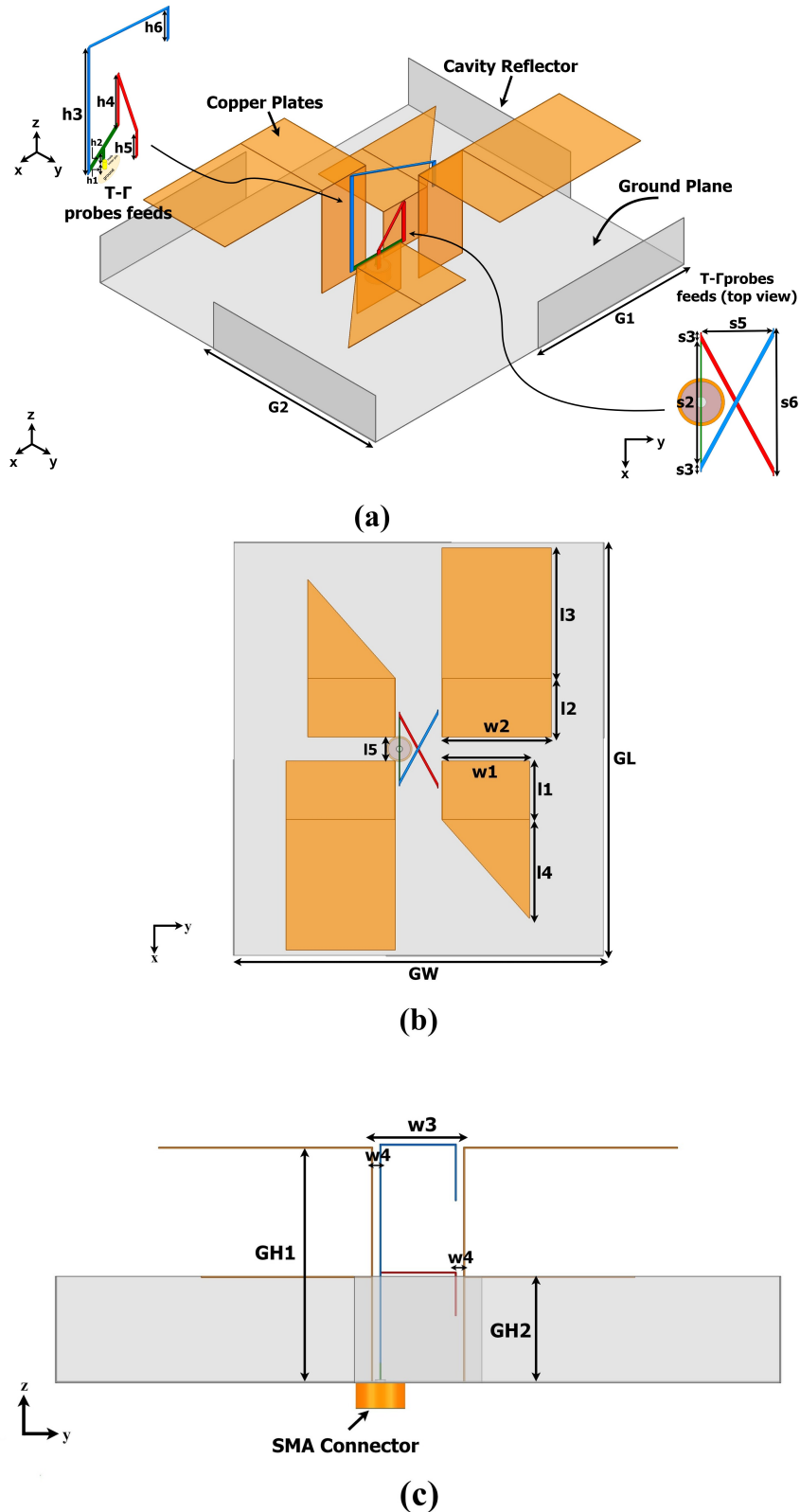


Fig. 1. (a) 3D design ME Antenna (b) top view antenna (c) Side view antenna.

As shown in Fig. 1 (a), the ME dipoles are connected in the center of the antenna ground plane so that both ME dipoles are separated by a distance of 11 mm. Each ME dipole antenna element consists of two vertical plates and two horizontal plates connected to the vertical plates. The vertical plates with heights of a quarter of a wavelength are short-circuited by the grounding of the reflector

cavity and are equivalent to magnetic dipoles, while the horizontal plates function as electric dipoles. To improve the AR bandwidth, the edges of the horizontal plates are chamfered at the smallest of the ME dipoles. In addition, four metal plates are added vertically to the edges of the ground, forming a cavity reflector with four gaps. As a result, not only can the AR bandwidth be greatly expanded, but lower back radiation can also be achieved.

The connection between the dipoles and the connector is made by coupling the proposed $T-\Gamma$ shaped power supply structure, as illustrated in Figure 1(a), a T-shaped structure has been proposed for the power supply which is connected directly to the SMA connector, note that there is a distance ($h_1 = 0.7$ mm) between the bottom of the pedestal and the ground plane of the cavity to avoid short-circuiting the SMA connector and divides the input power into two paths that interconnect two feed lines made of suspended copper sheet of different sizes due to the two dipole heights found in our antenna in a criss-cross fashion so that these Γ (gamma) shaped lines do not come into contact, in which they descend with sizes h_5 and h_6 and are fixed about 2 mm from the antenna's vertical magnetic dipole. Considering the impedance matching of the antenna, the horizontal branches of the two feed lines have the same sizes. The open vertical end of each feed line acts as a capacitor in which, by varying its length, we can adjust the antenna's impedance matching.

In order to achieve circular polarization performance, trapezoidal horizontal plates are chosen as electric dipole. The advantages of the trapezoidal plates compared to the rectangular plates are the S-parameter is better than with trapezoidal plates due that with this format we will have a better current impedance match due to the cut of the material.

Fig. 1 (b) shows the top view of the prototype. Meanwhile, Fig. 1 (c) shows a side view of the antenna, the overall volume of the proposed antenna is $190 \times 170 \times 55 \text{ mm}^3$. Details of the dimensions of the proposed antenna are shown in Table I.

B. Evolution and Parametric Study

To better understand the design of the proposed antenna, three ME CP dipole antenna structures were simulated, as shown in Fig. 2 (a), Fig. 2 (b) and Fig. 2 (c). Firstly, a ME dipole antenna was investigated, with only one ME dipole element and with a closed reflector cavity, we call it Ant 1 both horizontal plates were not chamfered, after which it was separated into two ME dipoles of the antenna, thus having two distinct bands, a much higher band polarized to the left and a lower band polarized to the right, as the interest is for the GNSS band, we focused on obtaining a better band polarized to the right in the order 1-2 Ghz, still the horizontal plates were not chamfered, we call this antenna Ant 2. Finally, we modified the walls of the reflector cavity in order to obtain gaps so that the impedance matching and the AR are adequate, we added chamfers to increase the AR in one of the ME dipoles for our proposed Antenna and compared its results.

TABLE I. SPECIFIED DIMENSIONS OF THE PRESENTED ANTENNA.

Parameters	GL	GW	GH_1	GH_2	G_1	G_2	l_1	l_2	l_3	l_4	l_5	w_1	w_2	w_3
Values/mm	190	170	55	25	90	100	27	27	60	40	11	40	50	22
Parameters	w4	s_1	s_2	s_3	s_4	s_5	s_6	s_7	h_1	h_2	h_3	h_4	h_5	h_6
Values/mm	2	11.5	13	2	2	17.4	34	2.5	0.7	4	51	21	10	13

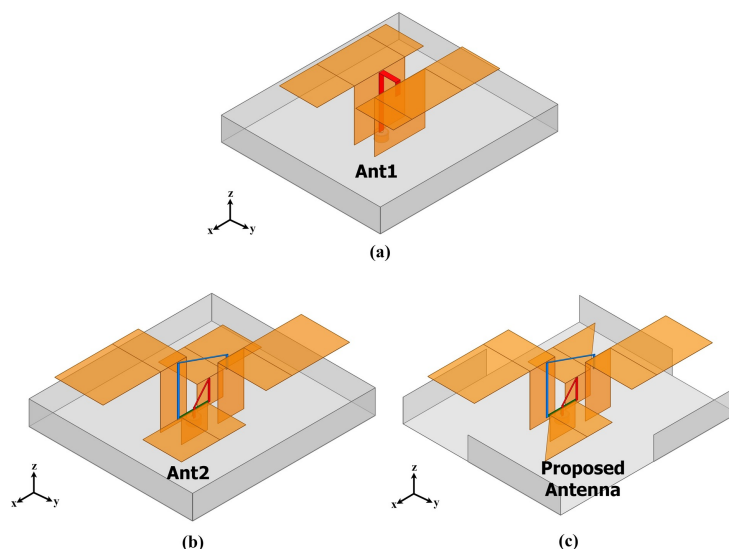


Fig. 2. Evolution of antenna models. (a) Ant1. (b) Ant2. (c) Presented Antenna.

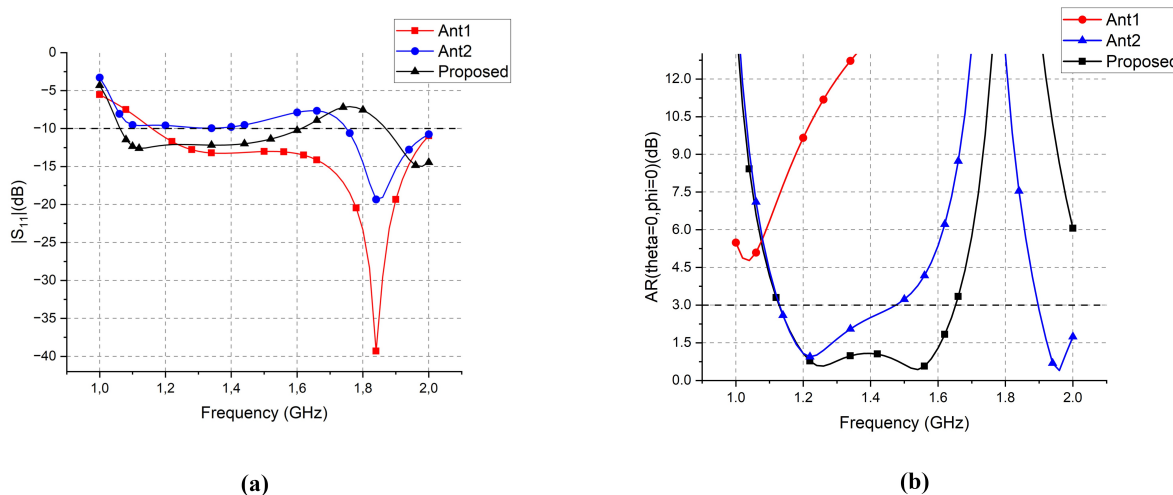


Fig. 3. The simulated results of Ant1, Ant2 and Proposed (a) $|S_{11}|$. (b) AR.

It can be noted that the AR parameter values for Ant1 are linearly polarized and do not meet the circular polarization requirement for operation in the GNSS band. As for Ant2, the AR values are attenuated due to the addition of the new feed form and the division into two ME dipoles. Finally, with various parameter settings and simulations, the $|S_{11}|$ and AR values fall within the GNSS band initially expected, as shown in Fig. 3 (a) and Fig. 3 (b).

To improve the performance of the CP, the shape and dimensions of the E-dipole were modified using imperfections (scraps or cuts) in the shape of the dipole, so the dimensions of the notches are obtained through various simulations and optimizations. A parametric analysis was carried out between parameters l_3 and l_4 with steps of ± 5 mm, to obtain an optimum value for the antenna, shown in Fig. 4.

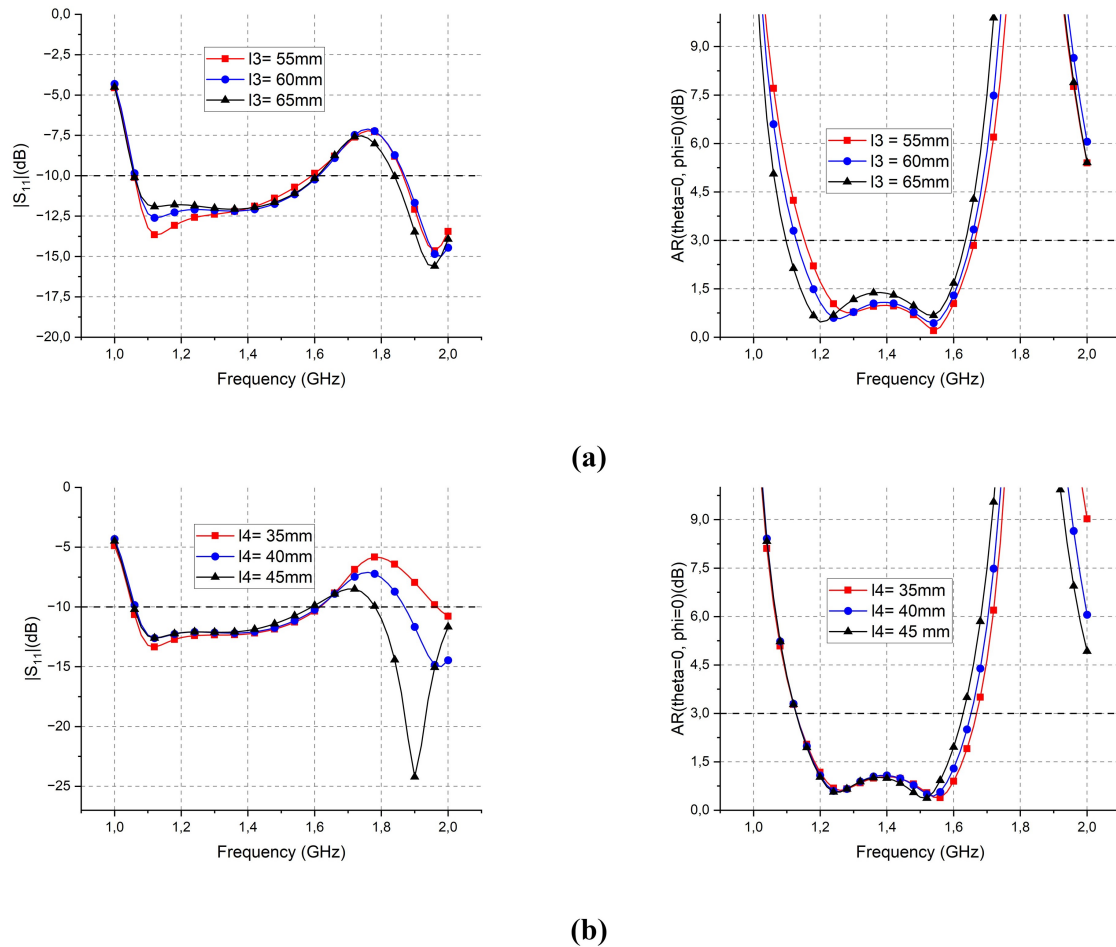


Fig. 4. Effects of E-dipole length on reflection coefficients and AR. (a) l_3 . (b) l_4 .

By analyzing Fig. 4 (a), it can be observed that when l_3 is increased we obtain a significant variation in the AR bandwidth, which is understood, causing a shift towards the desired area. Fig. 4 (b) shows that increasing l_4 leads to an increase in the AR bandwidth, while S_{11} shows no significant changes. This creates a point between the optimum, where $l_3 = 60$ mm and $l_4 = 40$ mm, which was chosen as the standard for our antenna. After the improvement through the parameterization of (l_3 and l_4), a $|S_{11}| < -10$ dB was obtained, from 1.03 to 1.61 GHz, and its bandwidth for axial ratio (AR) less than 3 dB, is 1.16 to 1.65 GHz, which comprises the entire GNSS band for both cases.

C. Distribution of Electric Field

In order to better explain the CP mechanism, we used the surface current distributions of the electric dipole at 1.17 GHz, 1.385 GHz and 1.57 GHz for different time phases of 0° , 90° , 180° and 270° , which are shown in Fig. 5, respectively.

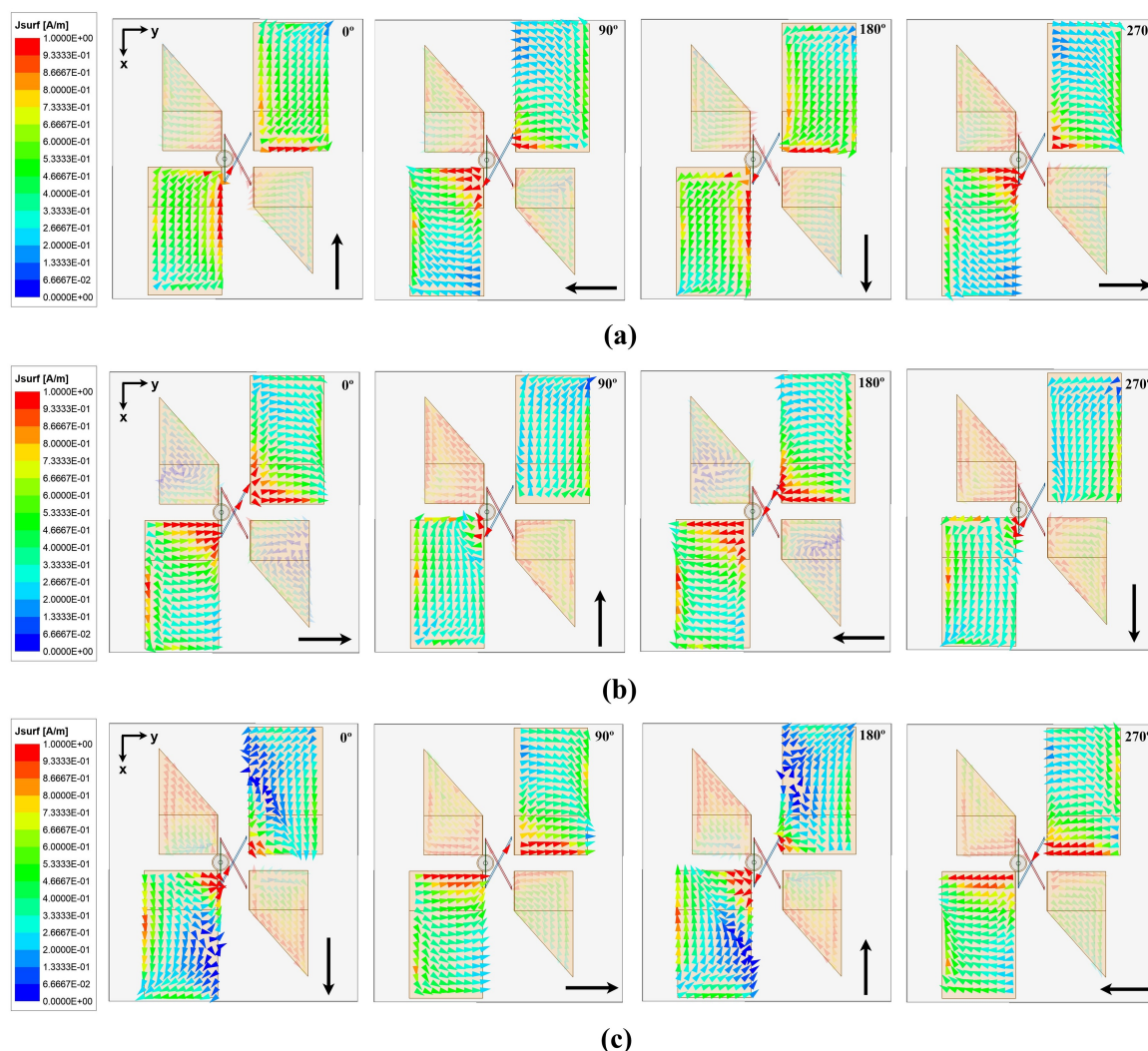


Fig. 5. Simulated surface current distributions at different time phases of 0° , 90° , 180° and 270° . (a) at 1.17 GHz. (b) at 1.385 GHz. (c) at 1.57 GHz.

To facilitate discussions and analysis in Fig. 5, we define the phase as 0° when the magnetic dipoles (larger and fewer vertical plates) have similar current distributions, and the observation points of the electric fields are defined as multiple wavelengths of the electric dipoles separated on the z-axis. The equivalent currents between two horizontal plates are represented as arrows to show the total current distributions on the cavity floor, in order to obtain a clear view.

As illustrated in Fig. 5 (a), Fig. 5 (b) and Fig. 5 (c), when the phase is equal to 0° , approximate open-loop currents are found along the short-circuited vertical plates and the ground, while the currents in the horizontal plates are relatively weak. Therefore, the electric fields at 1.17, 1.385 and 1.57 GHz point in the direction of the $-x$ axis, the $+y$ axis and the $+x$ axis respectively. When the phase is equal to 90° , the typical open current loops almost disappear due to the irregular current distributions in the vertical plates, and the currents in the horizontal plates reach a maximum. The electric field at the desired frequencies turns towards the $-y$ axis, $-x$ axis and $+y$ axis respectively. As already mentioned, when the phase is equal to 180° and 270° , the current distribution is similar to 0° and 90° with opposite current flow directions are obtained. Therefore, in these two cases, the electric field at the 3 desired frequencies points in the directions of the $+x$ axis, $-y$ axis and $-x$ axis for 180 degree and the $+y$ axis, $+x$ axis and $-y$ axis for 270 degree, respectively. Finally, the RHCP character is obtained as can be

seen by the large black arrows in the figures, respectively.

The physics behind of taking the different copper plates shapes is the horizontal branches of two T-Gamma power lines have the same size and geometry, but with different heights and the currents in the branches have the same direction of flow and approximate magnitude. Therefore, the horizontal branches can be equivalent to identical excitation sources in the same operating mode. In the case of the long E-dipole, the currents flow from one plate to the other. A current of approximately half a wavelength is obtained along the long E-dipole which generates the electric field in the -x direction when the phase is equal to 90° . The E field in the +x direction appears when the phase is equal to 270° . For the short E-dipole, the currents flow in the opposite direction as the large E-dipole. Two nulls are found on each horizontal plate. As mentioned earlier, the excitation sources at frequency operate in the same mode and therefore the excitation source at the has similar current magnitude and phase. Therefore, for the smaller E-dipole, when the phase is equal to 90° , the currents in each plate of the short E-dipole have the opposite current phase to that of the long E-dipole. In other words, an inverse current $I_e = -I_e$ is obtained in the short E-dipole. Next, the E field in the +x direction is generated. The E field in the -x direction appears when the phase is equal to 270° .

III. SIMULATED ANTENNA PERFORMANCE

A. Simulation of Axial ratio (AR), Realized Gain, Front to-back-ratio (FBR) and Radiation Efficiency

As shown in Fig. 6 (a) and Fig. 6 (b), the antenna's performance as a function of aperture (θ) shows that for both cases we will have an axial ratio of less than 3 dB at around 40 degrees and a gain of more than 2 dBi, as well as the maximum gain achieved by the antenna, which is 8.69 dBi. Fig. 7 (a) and Fig. 7 (b) shows the antenna's front-to-back-ratio (FBR), where the model shows an FBR greater than 20 dB difference between the right-hand circular polarization (RHCP) and left-hand circular polarization (LHCP) gains. which shows a low lower lobe pattern, as expected for a ME dipole antenna and the radiation efficiency was simulated, obtaining an efficiency greater than 90%.

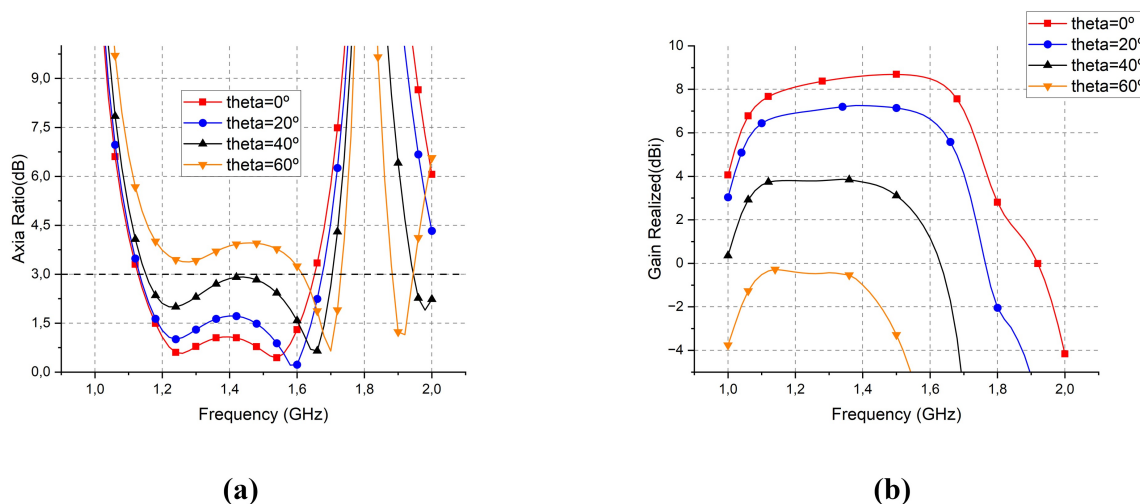


Fig. 6. Simulation of Axial Ratio (AR) and Gain values as a function of antenna aperture θ . (a) AR. (b) Realized gain.

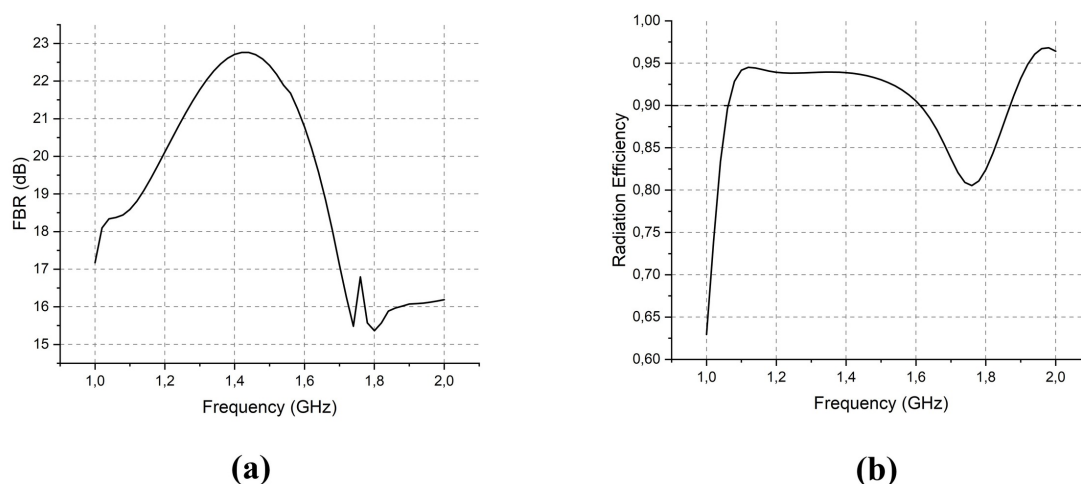


Fig. 7. Simulation results of (a) Front-to-Back-Ratio (FBR). (b) Radiation Efficiency.

B. Simulation Performance Applied to CubeSat

Fig. 8 shows the ME dipole antenna attached to the CubeSat 6U ($20\text{mm} \times 10\text{mm} \times 30\text{mm}$). We are interested in showing the performance of the antenna considering the entire operating structure, in this case the chassis of this nanosatellite, which was modeled in aluminum and simulated in ANSYS HFSS. Fig. 9 (a) shows the radiation pattern obtained for 1.57 GHz, which corresponds to the central frequency of the GPS L1, Beidou B1 and Galileo E1 bands. It can be seen that the maximum gain obtained considering the chassis losses is 8.57 dBi. In addition, in Fig. 9 (b) we can see some graphs relating to the antenna's performance. As expected, the impedance matching changes slightly for 1.57 GHz due to the chassis and the AR remains practically the same.

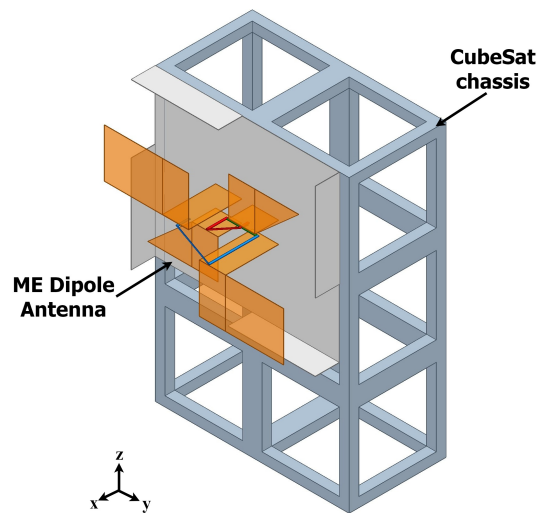


Fig. 8. ME Dipole antenna attached to the CubeSat 6U chassis.

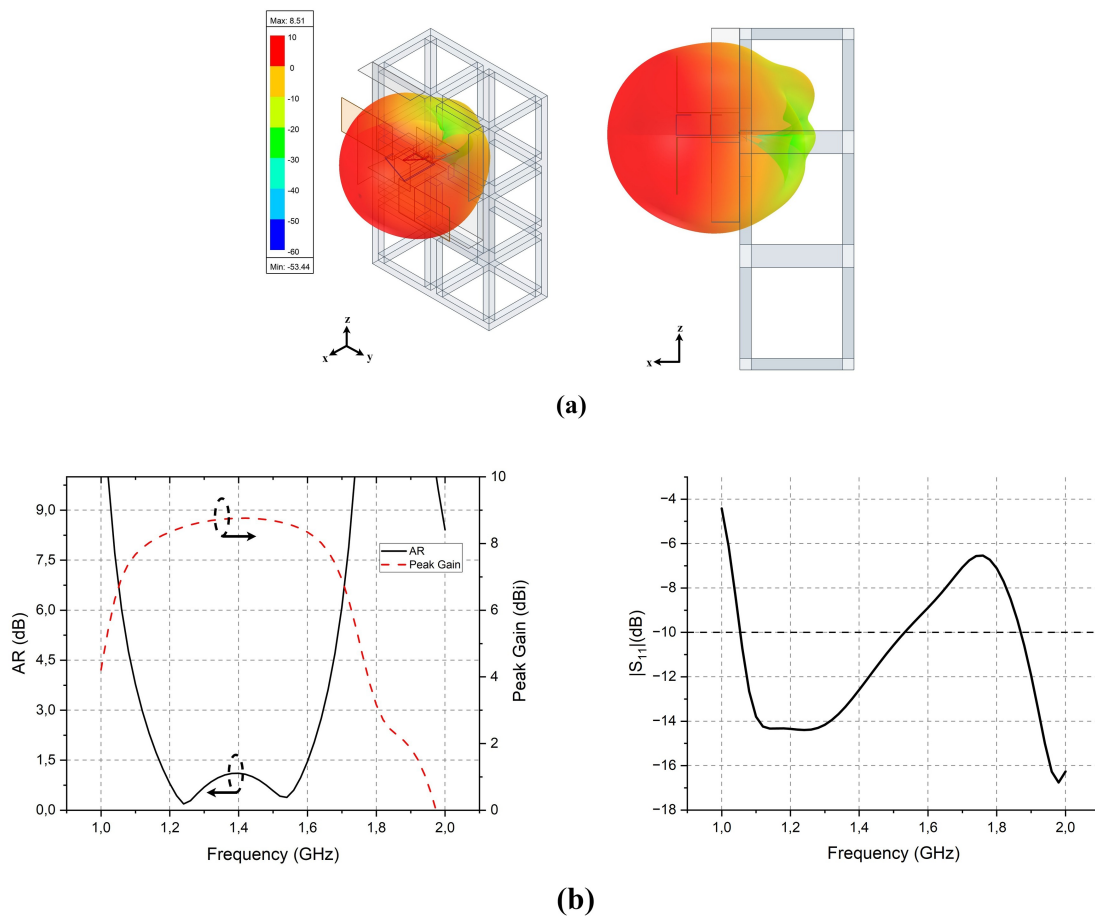


Fig. 9. Simulation results of the antenna coupled to the CubeSat. (a) Radiation pattern, scale 1:2. (b) Gain, AR and Return Loss.

IV. EXPERIMENTAL RESULTS AND COMPARISONS

The implementation of the ME dipole antenna is shown in Fig. 10 below. The prototype was made from copper material and measured in the laboratory in free space. The measured and simulated S-parameter (CST and ANSYS-HFSS) of the proposed ME dipole antenna is illustrated in Fig. 11 (a).

As seen in this figure, the measured frequency bandwidth is 1.13 GHz to 1.62 GHz with $S_{11} < -10$ dB, while the simulated one is 1.10 GHz to 1.66 GHz. The measured and simulated AR (CST and ANSYS-HFSS) is also shown in Fig. 11 (b). In this case, equation [1] from the following reference was used [18]. It can be seen that the bandwidth of the axial ratio is greater than the bandwidth of the input impedance. The measured 3 dB AR bandwidth is 1.10 to 1.63 GHz. Fig. 12 shows the simulated and measured radiation efficiency for the proposed antenna. In addition, due to the coupling losses of the cables used and the environment in which the setup was measured, there is a large variation in the measurement. In this case, equation [1] from the following reference was used [18]. The measured 3 dB AR bandwidth is 1.10 to 1.63 GHz. In addition, due to the coupling losses of the cables used, there is a large variation in the measurement.

$$AR = \sqrt{\frac{E_{x_o}^2 + E_{y_o}^2 + [E_{x_o}^4 + E_{y_o}^4 + 2E_{x_o}^2 E_{y_o}^2 \cos 2\Delta\phi]}{E_{x_o}^2 + E_{y_o}^2 - [E_{x_o}^4 + E_{y_o}^4 + 2E_{x_o}^2 E_{y_o}^2 \cos 2\Delta\phi]}} \quad (1)$$

Where $E_{x_o} = |S_{21}^{co}|$ and $E_{y_o} = |S_{21}^{cross}|$ are the transmission amplitudes of the co- and cross-polarizations, respectively, and $\Delta\phi = \angle S_{21}^{co} - \angle S_{21}^{cross}$ is the phase difference between them.

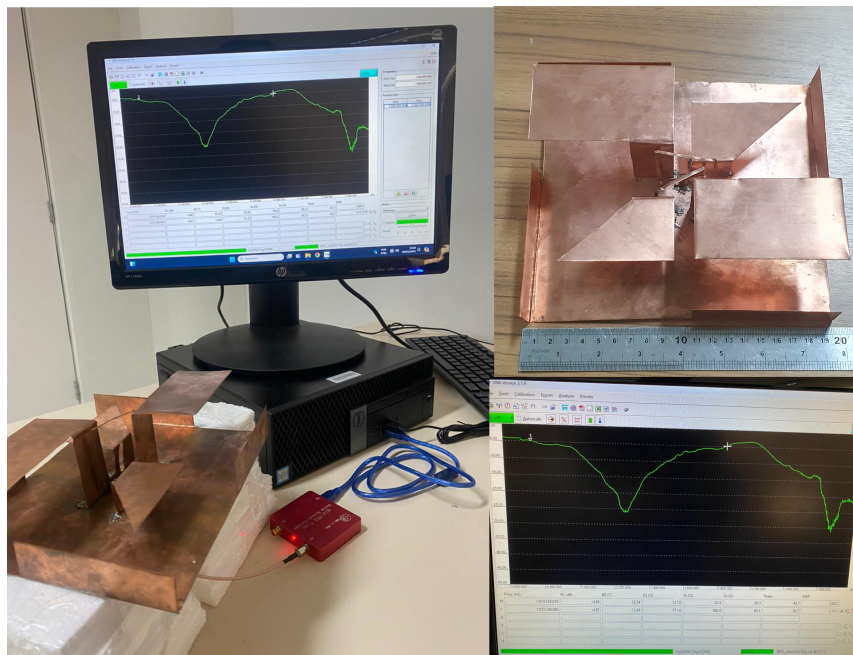


Fig. 10. Implementation of the proposed ME dipole antenna.

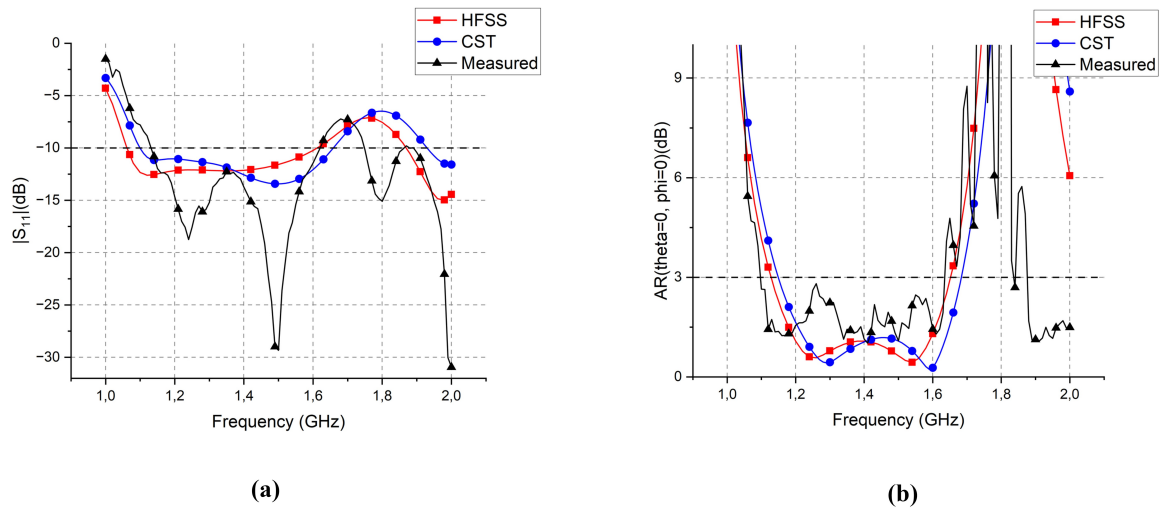


Fig. 11. Simulated and measured results of (a) $|S_{11}|$. (b) AR.

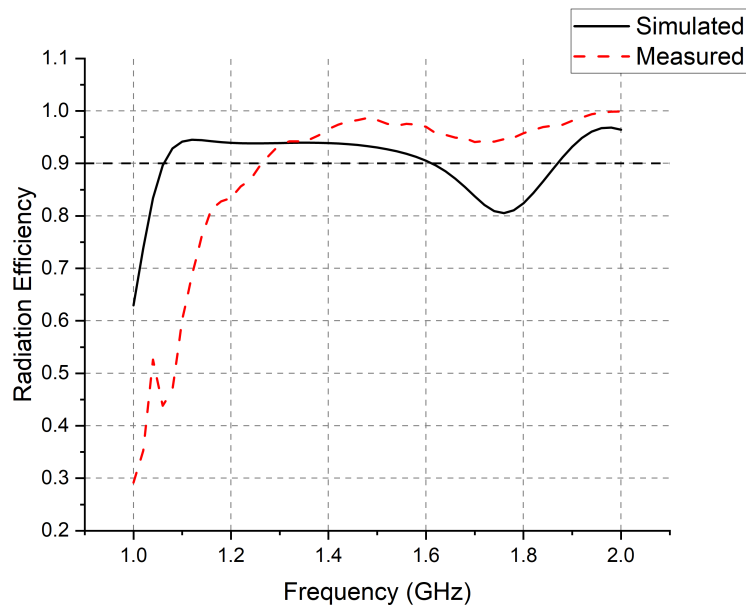


Fig. 12. Simulated and measured results of radiation efficiency.

Fig. 13 shows the measured and simulated gain and FBR in ANSYS-HFSS. The measured results are lower than the simulated ones due to manufacturing errors and environmental effects, however, these results are still satisfactory by practical standards. The measured maximum gain is 7.97 dBi at frequency of 1.238 GHz. In addition, the measured FBR is greater than 18 dB at frequencies from 1.17 GHz to 1.53 GHz, respectively.

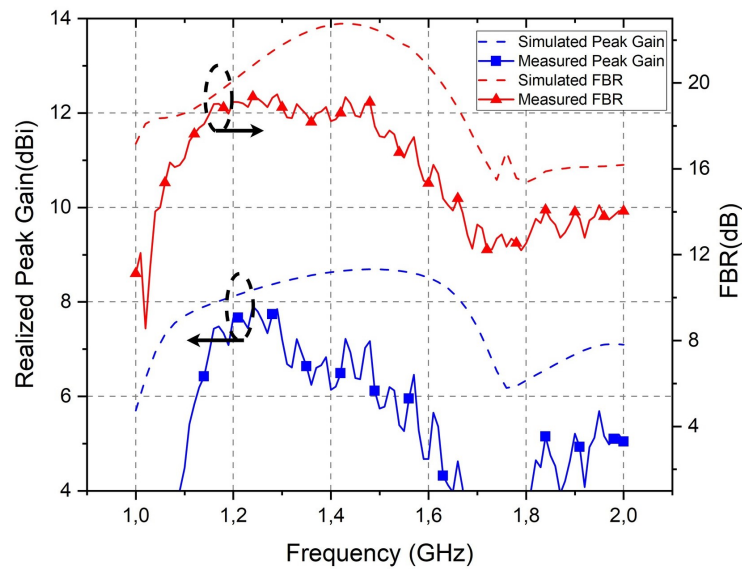


Fig. 13. Simulation and Measurement of realized peak gain and FBR.

The FBR was measured by analyzing the gain radiated in the forward direction (0 degrees relative to the transmitting antenna) compared to the gain radiated in the rearward direction of the antenna under test (180 degrees relative to the transmitting antenna). In this case, these gains were subtracted and the FBR was obtained. This parameter is relevant in directional antennas to determine the antenna's ability to focus the signal in the desired direction and reduce radiation in the opposite direction.

Fig. 14 (a) and Fig. 14 (b) show the measured and simulated radiation patterns in the E-plane and H-plane. Considering these graphs, low differences are observed between the simulated and measured RHCP. The tolerance between the simulated and measured LHCP is impressive, but it is a satisfactory result. In addition, Half Power Beam Widths (HPBWs) of 39.8° and 40.2° were obtained for the frequencies 1.17 GHz and 1.57 GHz respectively, which are appropriate for applications in the proposed GNSS band.

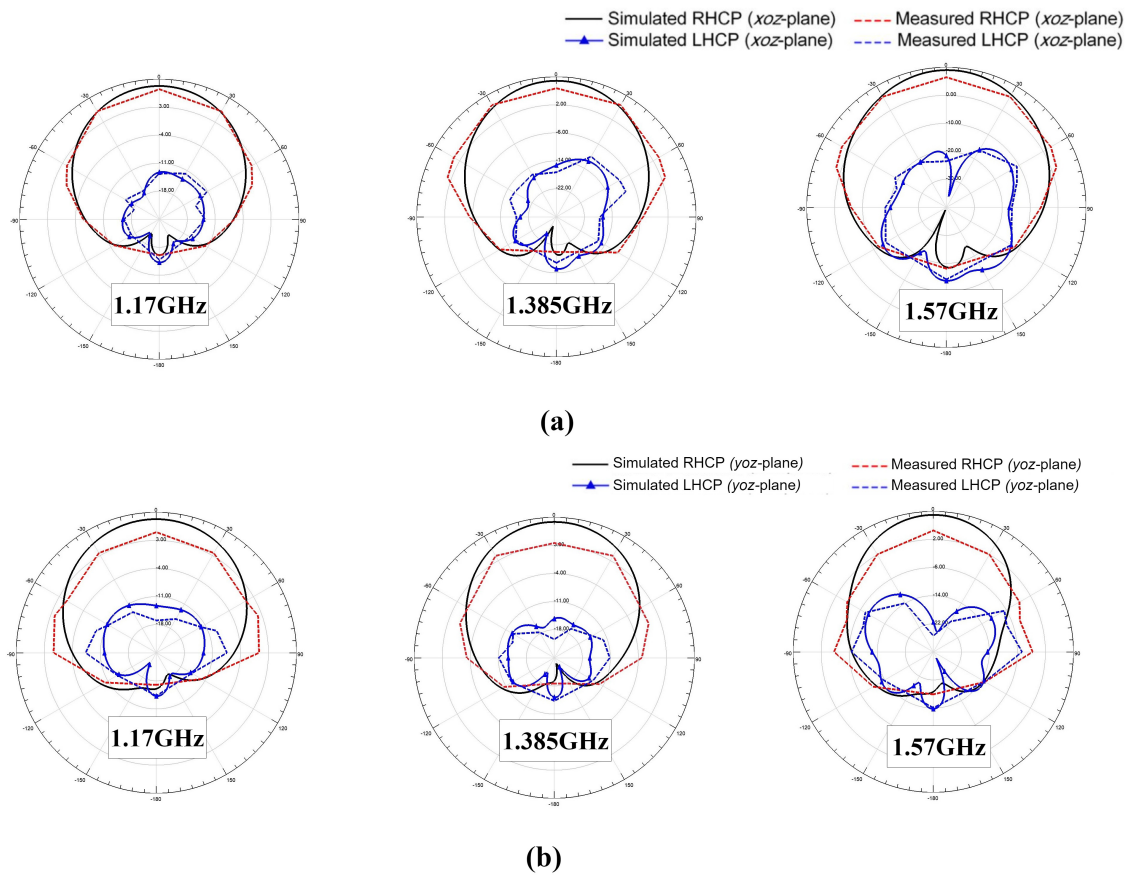


Fig. 14. Measured and simulated results of radiation patterns at 3 different frequencies in (a) E-Plane. (b) H-Plane.

Finally, a comparison was made between previous magnetolectric dipole antennas and the antenna proposed in this article, which have approximately the same structures and/or specifications, the results are shown in Table II. We note that the CP characteristic and the wide frequency bandwidth in [12], it has a lower gain in the frequency range of 1.5 to 2 GHz compared to the antenna proposed in this work. In addition, the ME CP dipole antenna proposed in [17] has satisfactory performance, but does not cover the GNSS band. We can conclude the antenna proposed in this article has a wider frequency bandwidth and benefits from the CP characteristic, as well as having a simpler structure and applied for cubesats equal to or superior to 6U.

TABLE II. COMPARISON BETWEEN THE PROPOSED ANTENNA AND PREVIOUS WORKS.

Ref.	Fc (GHz)	Antenna Size (λ_0^3)	Impedance Bandwidth	3dB AR Bandwidth	Peak Gain (dBi)	FBR (dB)	Antenna Structure	CubeSat
[17]	2.615	$1.607\lambda_0 \times 1.294\lambda_0 \times 0.267\lambda_0$	(1.76-3.46 GHz)	(1.68-3.55 GHz)	9.0	N/A	Simple	6U
[12]	2.15	$1.075\lambda_0 \times 1.075\lambda_0 \times 0.215\lambda_0$	(1.5-2.7 GHz)	(1.7-2.6 GHz)	6.2	>20	Simple	6U
[15]	2.775 and 5.15	$0.925\lambda_0 \times 0.925\lambda_0 \times 0.283\lambda_0$	(2.15–3.4 and 4–6.3 GHz)	(2.5-3.35 and 5-5.7 GHz)	8.0	>22	Simple	3U
[11]	1.385	$0.480\lambda_0 \times 0.480\lambda_0 \times 0.250\lambda_0$	(1.05-1.79 GHz)	(1.12-1.64 GHz)	6.9	>12	Simple	3U
[7]	1.385	$0.369\lambda_0 \times 0.369\lambda_0 \times 0.139\lambda_0$	(1.04-2.0 GHz)	(1.1-1.88 GHz)	4.0	N/A	Complex	3U
[14]	1.385	$0.614\lambda_0 \times 0.614\lambda_0 \times 0.139\lambda_0$	(0.98-1.64 GHz)	(1.16-1.65 GHz)	8.0	>16	Complex	3U
Proposed	1.385	$0.877\lambda_0 \times 0.785\lambda_0 \times 0.254\lambda_0$	(1.13-1.62 GHz)	(1.10-1.63 GHz)	8.69	>20	Simple	6U

V. CONCLUSIONS

This paper presents a wideband ME dipole antenna with circular polarization and compact dimensions of $190 \times 170 \times 55 \text{ mm}^3$. The antenna integrates M-dipole and E-dipole antennas in parallel, with adjacent E-dipoles in opposite directions and one of them chamfered in order to improve the AR. A crossed feeding T- Γ -shaped line was designed to efficiently excite the antenna. The prototype was fabricated, measured and operated in the 1.13-1.62 GHz range for impedance matching, with an AR RHCP bandwidth of 1.10-1.63 GHz. Using a cavity reflector with defected sidewalls, we achieved a front-to-back ratio of more than 20 dB and an average gain of 8 dBi. The proposed antenna exhibits unidirectional radiation patterns and radiation efficiency above 90%, suggesting potential use in global navigation satellite systems (GNSS).

ACKNOWLEDGMENTS

This study was financed in part by the Coordenação de Aperfeiçoamento de Pessoal de Nível Superior - Brasil (CAPES) – Finance Code 001 and Federal University of Rio Grande do Norte (UFRN).

REFERENCES

- [1] K. M. Luk, H. Wong, "A new wideband unidirectional antenna element," *International Journal of Microwave and Optical Technology*, vol. 1, pp. 35–44, 2006.
- [2] X. Zhang, Y. Jiao, Y. Gao, S. Sun, Y. Zhang, "A wideband circularly polarized directional magnetoelectric dipole antenna," *2019 International Conference on Microwave and Millimeter Wave Technology (ICMMT)*, pp. 1–3, 2019.
- [3] M. Han, W. Dou, "A broadband circular polarized magneto-electric dipole antenna," *2018 International Conference on Microwave and Millimeter Wave Technology (ICMMT)*, pp. 1–3, 2018.

- [4] M. F. Bolster, "A new type of circular polarizer using crossed dipoles," *IRE Transactions on Microwave Theory and Techniques*, vol. 9, p. 385–388, 1961.
- [5] M. Han, W. Dou, "Low profile broadband circularly polarized magnetolectric dipole antenna with short-circuit patch for wireless communication," *Microwave and Optical Technology Letters*, vol. 62, p. 1307–1314, 2020.
- [6] H.-G. Xue, L.-F. Li, X.-X. Yang, Z. Ma, J.-Y. Mo, "A wideband circular polarization quasi magnetic-electric dipole antenna with single feed," *2016 IEEE MTT-S International Conference on Numerical Electromagnetic and Multiphysics Modeling and Optimization (NEMO)*, pp. 1–3, 2016.
- [7] H. Zhang, Y. Guo, G. Wang, "A design of wideband circularly polarized antenna with stable phase center over the whole gnss bands," *IEEE Antennas and Wireless Propagation Letters*, vol. 18, p. 2746–2750, 2019.
- [8] M. Li, K.-M. Luk, L. Ge, K. Zhang, "Miniaturization of magnetolectric dipole antenna by using metamaterial loading," *IEEE Transactions on Antennas and Propagation*, vol. 64, p. 4914–4918, 2016.
- [9] Y. Xu, M. Zhou, A. Wang, J. Hou, "Design of a compact magneto-electric dipole antenna," *Microwave and Optical Technology Letters*, vol. 65, p. 2331–2336, 2023.
- [10] D.-C. Chang, H.-J. Lee, "A wideband circularly polarized antenna for gnss," *2016 IEEE 5th Asia-Pacific Conference on Antennas and Propagation (APCAP)*, pp. 343–344, 2016.
- [11] H. Tran, S. X. Ta, I. Park, "Single-feed, wideband, circularly polarized, crossed bowtie dipole antenna for global navigation satellite systems," *Journal of Electromagnetic Engineering and Science*, vol. 14, p. 299–305, 2014.
- [12] P. Mohammadi, M. Rezvani, T. Siah, "A circularly polarized wide-band magneto-electric dipole antenna with simple structure for bts applications," *International Journal of Electronics and Communications*, vol. 105, p. 92–97, 2019.
- [13] J. J. H. Wang, "Antennas for global navigation satellite system (gnss)," *Proceedings of the IEEE*, vol. 100, p. 2349–2355, 2012.
- [14] S. Fu, X. Zhao, C. Li, Z. Wang, "Broadband circularly polarized tapered dipole antenna for gnss applications," *International Journal of RF and Microwave Computer-Aided Engineering*, vol. 32, p. e23367, 2022.
- [15] J. Tao, Q. Feng, "Dual-band magnetolectric dipole antenna with dual-sense circularly polarized character," *IEEE Transactions on Antennas and Propagation*, vol. 65, p. 5677–5685, 2017.
- [16] M. Shokri, C. Ghobadi, J. Nourinia, "Dual-band circularly polarized asymmetric dipole array antenna for gps 11 and 12 bands," *International Journal of Electronics and Communications*, vol. 169, p. 154753, 2023.
- [17] K. Kang, Y. Shi, C.-H. Liang, "A wideband circularly polarized magnetolectric dipole antenna," *IEEE Antennas and Wireless Propagation Letters*, vol. 16, p. 1647–1650, 2017.
- [18] X. You, R. T. Ako, W. S. L. Lee, M. Bhaskaran, S. Sriram, C. Fumeaux, W. Withayachumnankul, "Broadband terahertz transmissive quarter-wave metasurface," *APL Photonics*, vol. 5, p. 096108, 2020.
- [19] C.-Q. Feng, F.-S. Zhang, H.-J. Zhang, J.-X. Su, "A single-feed circularly polarized magnetolectric dipole antenna for wideband wireless applications," *Progress In Electromagnetics Research M*, vol. 65, p. 1–8, 2018.
- [20] D. Yang, K. Xue, H. Zhai, "A wideband circularly polarized magneto-electric dipole antenna," *2018 International Conference on Microwave and Millimeter Wave Technology (ICMMT)*, pp. 1–3, 2018.
- [21] Y.-Q. Zhang, X. Li, L. Yang, S.-X. Gong, "Dual-band circularly polarized annular-ring microstrip antenna for gnss applications," *IEEE Antennas and Wireless Propagation Letters*, vol. 12, p. 615–618, 2013.
- [22] S. Jović, M. Clénet, Y. A. M.M., "Novel wideband antenna for gnss and satellite communications," *2020 14th European Conference on Antennas and Propagation (EuCAP)*, pp. 1–5, 2020.